

ISOBARIC RECONSTRUCTION OF THE BARYONIC ACOUSTIC OSCILLATION

XIN WANG^{1,10}, HAO-RAN YU^{1,2}, HONG-MING ZHU^{3,4}, YU YU⁵, QIAOYIN PAN⁹, UE-LI PEN^{1,6,7,8}

Draft version November 8, 2018

ABSTRACT

In this paper, we report a significant recovery of the linear baryonic acoustic oscillation (BAO) signature by applying the isobaric reconstruction algorithm to the non-linearly evolved matter density field. Assuming that only the longitudinal component of the displacement is cosmologically relevant, this algorithm iteratively solves the non-linear coordinate transform between the Lagrangian and Eulerian frames without requiring any specific knowledge of the dynamics. For dark matter field, it produces the non-linear displacement potential with very high fidelity. The reconstruction error at the pixel level is within a few percent caused only by the emergence of the transverse component after the shell-crossing. As this method circumvents one of the most strongest non-linearity in density field, the reconstructed field is well-described by linear theory and is immune from the bulk-flow smearing of the BAO signature, and therefore could be used to significantly improve the precision of measuring the sound horizon scale s . For a perfect large-scale structure survey at redshift zero without Poisson or instrumental noise, the fractional error $\Delta s/s$ is reduced by a factor of ~ 2.7 , and is very close to the ideal limit one would ever achieve with linear power spectrum and Gaussian covariance matrix.

Keywords: large-scale structure of universe

1. INTRODUCTION

The large-scale structure (LSS) surveys provide a wealth of cosmological information of our Universe. Particularly, the wiggling feature of the baryonic acoustic oscillation imprinted in the matter power spectrum encodes the characteristic scale of sound horizon $s \sim 100\text{Mpc}/h$, which serves as a standard ruler and a robust method for measuring the cosmological distance (Eisenstein 2003; Blake & Glazebrook 2003; Hu & Haiman 2003; Seo & Eisenstein 2003). Since its first detection in SDSS by Eisenstein et al. (2005), BAO has then become essential for almost all ongoing and future LSS surveys. Despite the fact that s being relatively large, as the Universe evolves, its measurement accuracy from the power spectrum (or two-point correlation function) starts to decrease rather rapidly due to the non-linear gravitational effect. Statistically, the information leaks into higher order statistics, e.g. bispectra or trispectra etc.,

as the fields become more and more non-Gaussian with increased variance. This could be seen from the measurement of the so-called Fisher information, as a plateau would appear at quasi-linear regime where the BAO feature resides (Rimes & Hamilton 2005, 2006). Meanwhile, the same structure formation process would move galaxies away from their initial locations, and erase this feature encoded initially (Crocce & Scoccimarro 2008). Eventually, one starts to lose the constraining power on cosmology due to the combined effect of non-Gaussianity and the degraded BAO signal (Seo & Eisenstein 2007; Ngan et al. 2012).

This situation then leads to numerous efforts to reconstruct the BAO signature and improve the measurement precision of the sound horizon scale from LSS. For example, a logarithmic transformation or Gaussianization processes seem to improve the non-Gaussianity and bring back some information leaked into higher order statistics (Weinberg 1992; Neyrinck 2011). On the other hand, Eisenstein et al. (2007) (hereafter ZA reconstruction) first demonstrated that it is possible to sharpen the BAO peak in the correlation function and improve the measurement accuracy. This simple yet powerful algorithm has since then be improved and applied to real measurement (Padmanabhan et al. 2012; Mehta et al. 2012). Meanwhile, as the physical picture starts to clarify, more algorithms emerge (Tassev & Zaldarriaga 2012b; Schmittfull et al. 2015).

Historically, the attempt to undo the non-linear structure formation process dates far back before these efforts. Peebles (1989, 1990) first applied the principle of least action to reconstruct the trajectories of Local Group. This technique was then further developed by other authors (Croft & Gaztanaga 1997; Brenier et al. 2003) but without any application to cosmology due to its computational cost. On the other hand, various dynamical approaches were trying to inverse the dynamical system without any decaying modes so that

¹ Canadian Institute for Theoretical Astrophysics, 60 St. George St., Toronto, ON, M5H 3H8, Canada

² Kavli Institute for Astronomy and Astrophysics, Peking University, Beijing 100871, China

³ Key Laboratory for Computational Astrophysics, National Astronomical Observatories, Chinese Academy of Sciences, 20A Datun Road, Beijing 100012, China

⁴ University of Chinese Academy of Sciences, Beijing 100049, China

⁵ Key Laboratory for Research in Galaxies and Cosmology, Shanghai Astronomical Observatory, Chinese Academy of Sciences, 80 Nandan Road, Shanghai 200030, China

⁶ Dunlap Institute for Astronomy and Astrophysics, University of Toronto, 50 St. George Street, Toronto, Ontario M5S 3H4, Canada

⁷ Canadian Institute for Advanced Research, CIFAR Program in Gravitation and Cosmology, Toronto, Ontario M5G 1Z8, Canada

⁸ Perimeter Institute for Theoretical Physics, 31 Caroline Street North, Waterloo, Ontario, N2L 2Y5, Canada

⁹ School of Physics, Nankai University, 94 Weijin Rd, Nankai, Tianjin, 300071, China

¹⁰ xwang@cita.utoronto.ca

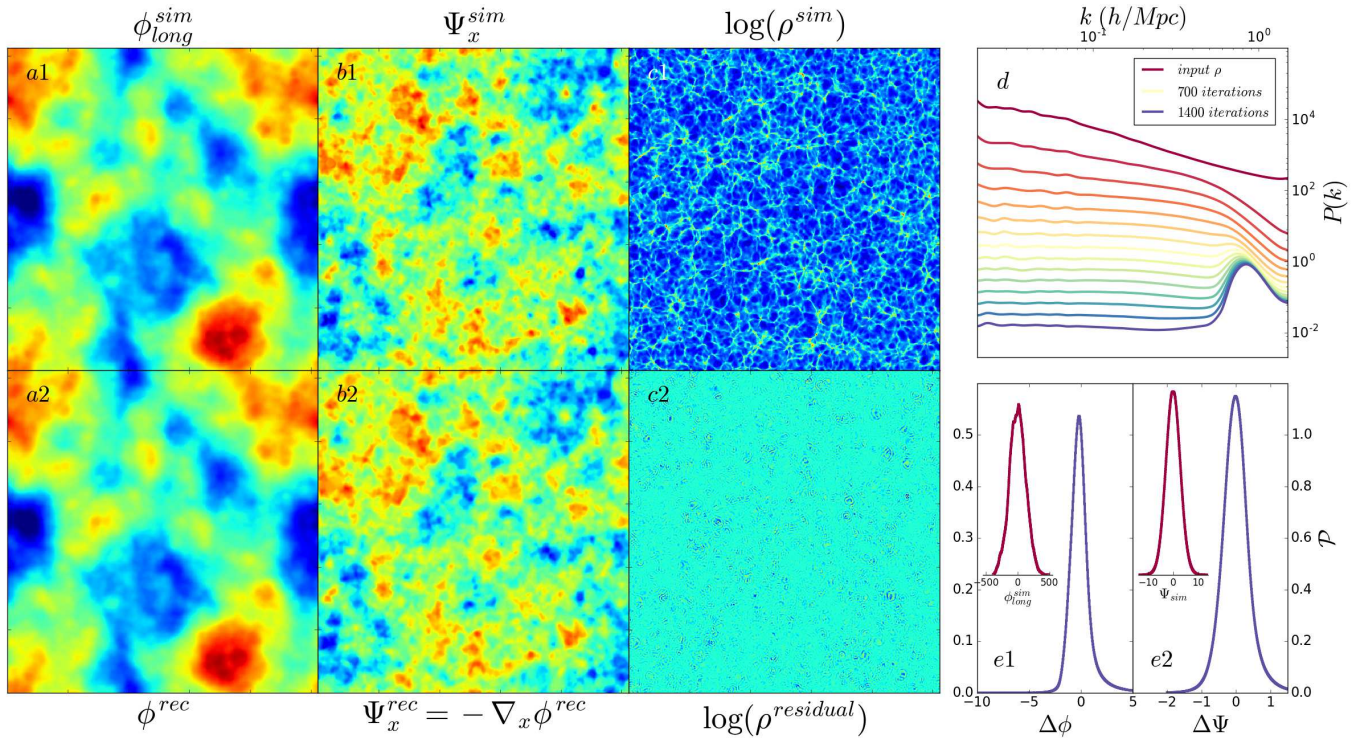


Figure 1. (Left six panels): The visual comparison of N-body simulation (*top row*) and the isobaric reconstruction (*bottom row*). From left to right, we show the displacement potential ϕ (panel *a1* and *a2*), the x component of the displacement field (panel *b1* and *b2*), the logarithmic of density field (*c1*) and the residual density map after 1400 iterations (*c2*). The same color scheme is applied among simulated and reconstructed field for *a* and *b* panels. (Right three panels): Statistical properties of the reconstruction, including the power spectra of the residual density field after many iterations (*d*); and the histograms of the reconstruction error $\Delta\phi = \phi_{long}^{sim}(\mathbf{q}) - \phi^{rec}(\xi)$ (*e1*) and $\Delta\Psi = \Psi_i^{sim}(\mathbf{q}) - \Psi_i^{rec}(\xi)$ (*e2*) at the pixel level.

observational errors will not overpower the real initial fluctuations (Nusser & Dekel 1992; Gramann 1993; Narayanan & Croft 1999). Meanwhile, as the computational processing power increases steadily in recent years, there are also attempts to directly sample all possible initial states by Markov Chain Monte Carlo method with fast forward model (Wang et al. 2013). Unlike most previous works, Eisenstein et al. (2007) tried to recover the linear power spectrum instead of initial density distribution, which is almost uniform, $\delta_\rho \ll 1$, and therefore practically much more challenging.

From the perspective of Lagrangian dynamics, the strong non-linearity presented in the density field δ_ρ is attributed to both the gravitational evolution of the particle movement, manifested by the non-linear displacement $\Psi(\mathbf{q}) = \mathbf{x} - \mathbf{q}$ of particles, and the coordinate transform between Lagrangian and Eulerian frame, where \mathbf{x} and \mathbf{q} are the Eulerian and Lagrangian position respectively. With the assumption of the mass conservation and a uniform matter distribution at the initial state, this coordinate transform could simply be expressed as

$$\det\left(\frac{\partial x_i}{\partial q_j}\right) = \det(\delta_{ij} + \partial_i \Psi_j) = \frac{\bar{\rho}}{\rho} = \frac{1}{1 + \delta_\rho}. \quad (1)$$

Recently, one starts to realize that equation (1) is the major source of various theoretical and practical difficulties encountered in the large-scale structure measurement (Tassev & Zaldarriaga 2012a,b). Therefore, by avoiding this extra non-linearity, the displacement field itself would be less non-linear and much easier to handle theoretically. Of course, by definition, $\Psi(\mathbf{q})$ is not an ob-

servable as it involves the unknown initial location \mathbf{q} . As a result, there have been efforts concentrating on the statistical extraction of $\Psi(\mathbf{q})$, e.g. the maximum likelihood method by Tassev & Zaldarriaga (2012b).

In principle, given a non-linear density map δ_ρ , and assuming that only the longitudinal component of the displacement field, i.e. $\Psi = -\nabla\phi$, is cosmologically relevant, equation (1) reduces to the so-called elliptical Monge-Ampère equation and becomes solvable with appropriate boundary condition¹¹. If the input density map δ_ρ is generated from particles movement without any crossing nor rotation, i.e. no transverse component of $\Psi(\mathbf{q})$, the recovered solution would be exactly the one we desire. In reality, however, these transverse components do emerge, but only at smaller scales (Chan 2014). Therefore the resultant reconstruction error in the BAO regime is negligible. Recently, Zhu et al. (2016) first proposed to apply the *potential isobaric reconstruction* algorithm to solve equation (1) for the displacement potential ϕ , and demonstrated the high correlation with initial density field, while Pan et al. (2016) showed that the Fisher information of the reconstructed field are significantly increased especially at quasi-linear regime, and then Yu et al. (2017) studied for halo density field.

In this paper, we apply the same algorithm and par-

¹¹ The existence and uniqueness of the solution to the Monge-Ampère equation is out of the scope of this paper. It was proven by Bakelman (1957); Aleksandrov (1958) for the generalized solution with Dirichlet boundary condition and Lions et al. (1986) for the Neumann problem. One could also see e.g. Trudinger & Wang (2008) for more detailed discussion.

ticularly concentrate on the improvement of cosmological information from measuring the baryonic acoustic oscillation. In section 2., we first review this algorithm and demonstrate their ability to recover the non-linear displacement field. We focus on the BAO signature in section 3., and show the recovered wiggles and improved accuracy in cosmological measurement. Finally, we conclude and discuss in section 4. Throughout this paper, the N-body simulations were run with numerical code CUBE, with the box size of 1024 Mpc/h, and 512^3 particles. We adopt the Planck 2015 results (Planck Collaboration et al. 2016) as our fiducial cosmological parameters.

2. THE POTENTIAL ISOBARIC RECONSTRUCTION

As a non-linear partial differential equation, the numerical solution to equation (1) is nontrivial. Even though various numerical strategies, e.g. Zeligovsky et al. (2010); Liu et al. (2014), do exist in literatures, the major challenge for the cosmological application here is the frame mismatch between the Lagrangian gradient of the displacement $\partial_i \Psi_j = \partial \Psi_i / \partial q_j$ and the Eulerian density field ρ . In this paper, we follow the multi-grid algorithm proposed by Pen (1995, 1998) to iteratively solve the differential form of this mass conservation equation in a moving curvilinear coordinate system, which we name as the *potential isobaric coordinate*.

To present our numerical algorithm, we simply take the differentiation of equation (1) with respect to some time-like iteration parameter τ , and obtain the conservation equation

$$d_\tau \left[\rho(\mathbf{x}(\mathbf{q})) \det \left(\frac{\partial x_i}{\partial q_j} \right) (\mathbf{q}) \right] = 0 \quad (2)$$

of a unit Lagrangian volume. For a fixed Eulerian fluid element, however, it further simplifies to $d_\tau \rho = 0$. Notice that both equations (1) and (2) are expressed locally, and do not care about any particular path of maintaining the conservation, as long as the density and volume of given fluid element vary consistently. However, from the field's perspective, equation (2) is nothing but the continuity equation with respect to parameter τ . Following the same notation of Pen (1995, 1998), in a curvilinear coordinate $\boldsymbol{\xi} = \{\xi_\mu\} = \{\xi_1, \xi_2, \xi_3\}$, we adopt the following ansatz for the coordinate transform at each iteration step

$$x^i = \xi^\mu \delta_\mu^i + dx^i = \xi^\mu \delta_\mu^i + \frac{\partial(d\phi)}{\partial \xi^\nu} \delta^{\nu i}, \quad (3)$$

where $d\phi$ is the increment of the displacement potential. As demonstrated by Pen (1998), in the isobaric frame, i.e. the mass per volume element is kept constant, the continuity equation could be expressed as a linear elliptic equation

$$\partial_\mu (\rho \sqrt{g} e_i^\mu \delta^{i\nu} \partial_\nu (d_\tau \phi)) = \partial_\mu (\rho \sqrt{g} e_i^\mu (d_\tau x^i)) = d_\tau \rho, \quad (4)$$

where the dreibein e_i^μ is the inverse of the triad, or the Jacobian matrix, $e_i^\mu = \partial x^i / \partial \xi^\mu$, the volume element $\sqrt{g} = \det(e_i^\mu)$. For given non-linear density map $\rho(\mathbf{x})$, we would like to reverse the frame deformation, and solve for the increment of displacement potential $d\phi$, where

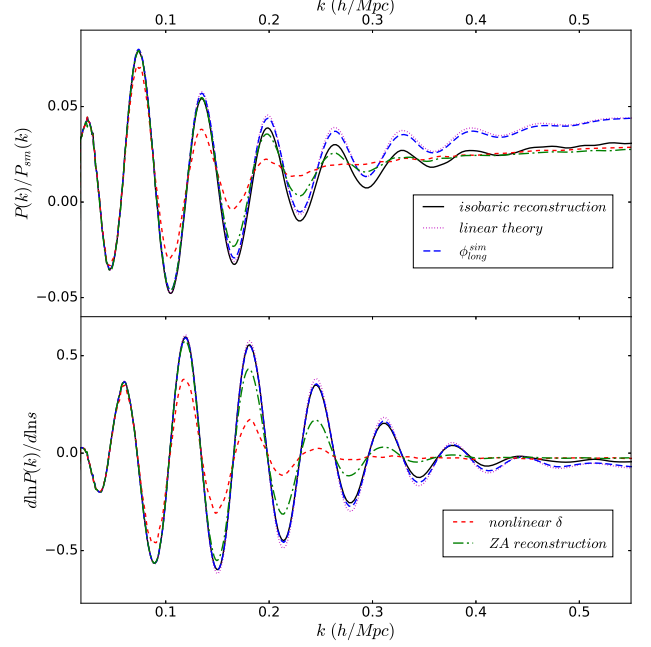


Figure 2. Comparison of BAO signature (*upper*) and the dependence of the power spectra with respect to the sound horizon s scale (*lower*) at redshift $z = 0$. To eliminate the sample variance, we run a few N-body simulations and reconstructions with different transfer functions (with different assumptions of BAO) but the same initial random seeds. For ZA reconstruction (Eisenstein et al. 2007), we assume a Gaussian smoothing with $R = 15$ Mpc/h.

$d\phi = d_\tau \phi d\tau = d_\tau \phi$ with the assumption that $d\tau = 1$ since we are free from parametrizing τ . As shown in Zhu et al. (2016), this is done by substituting $d\rho$ in equation (4) with the negative non-linear density contrast $-\Delta\rho = \bar{\rho} - \sqrt{g}\rho$ together with a spatial smoothing S to ensure the smallness of the resultant $d\phi$, i.e.

$$\partial_\mu (\rho \sqrt{g} e_i^\mu \delta^{i\nu} \partial_\nu (d\phi)) = S(-\Delta\rho + C + E), \quad (5)$$

here C and E are the compression and expansion limiters for improving the numerical stability (Pen 1998). Consequently, the triad e_μ^i would always be kept as positive definite. After moving the grid with equation (3), we estimate the density increment $d\rho$ from equation (4) and then repeat equation (5) with re-evaluated density contrast $\rho^{(i+1)} = \rho^{(i)} + d\rho^{(i)}$.

Eventually, the reconstructed displacement potential is simply a summation of all iterations,

$$\phi^{rec}(\boldsymbol{\xi}) = \sum_i^{iters} d\phi^{(i)}(\boldsymbol{\xi}^{(i)}(\boldsymbol{\xi})), \quad (6)$$

here we have explicitly denoted the *one-to-one* mapping between the intermediate and final coordinate $\boldsymbol{\xi}^{(i)}(\boldsymbol{\xi})$, which is only possible because of the positive definiteness of the transform matrix e_μ^i we achieved in solving equation (5). As a result, our final product ϕ^{rec} is then charted in a frame $\boldsymbol{\xi}$ that would be almost identical to the theoretically defined Lagrangian coordinate \mathbf{q} , and we will have $\phi^{rec}(\boldsymbol{\xi}) \approx \phi_{long}^{sim}(\mathbf{q})$ at the *pixel level*.

In the first column of Figure 1., i.e. panel a1 and a2 (with the same colorbar), one could see that this is indeed the case. The simulated displacement potential ϕ_{long}^{sim} (panel a2) is simply calculated by taking the longi-

tudinal component of the real displacement. The visual difference is not very obvious even if we compare with the full displacement vector field, i.e. Ψ_x^{sim} (panel b1) versus $\Psi_x^{rec} = -\nabla_x \phi^{rec}$ (panel b2), when transverse contribution starts to emerge after the shell-crossing. As shown in the histogram of $\Delta\phi = \phi_{long}^{sim}(\mathbf{q}) - \phi^{rec}(\xi)$ (panel e1), the reconstruction error is within a percent level for ϕ^{rec} , and roughly ten-percent level for displacement Ψ itself (panel e2).

In panel c1 and c2 of Figure 1., we also display a visual comparison between the input density map and its residual after 1400 iterations. As one could see, the non-vanishing residuals are basically around high density region, where the displacement field Ψ would no longer be captured only by longitudinal component, $-\nabla\phi$, anymore. As shown from the power spectra of the residual map in panel d, this starts to occur around the comoving Fourier scale $k \gtrsim 0.6h/\text{Mpc}$ and peaks around $0.8h/\text{Mpc}$, where although the large scale power eventually decays to about six orders of magnitude smaller compared to the input, small-scale power is still around unity.

3. MEASURING THE BARYONIC ACOUSTIC OSCILLATION

We are particularly interested in applying this isobaric reconstruction algorithm to detect the BAO signature in the power spectrum. As demonstrated by various authors, e.g. Crocce & Scoccimarro (2008), in the nonlinear density field, the sharp BAO features from the initial fluctuation $P_{ini}(k)$ is smeared out by the bulk flow of the galaxies even at the relatively large BAO scale. This could be seen by simply expressing the nonlinear density δ_ρ from the continuity equation (1) in Fourier space, and then taking the ensemble average, so the nonlinear power spectra reads (Crocce & Scoccimarro 2006, 2008)

$$P_{nl}(k) = \int \frac{d^3r}{(2\pi)^3} e^{i\mathbf{k}\cdot\mathbf{r}} [\langle e^{i\mathbf{k}\cdot\Delta\Psi} \rangle - 1] \\ = G^2(k)P_{ini}(k) + P_{mc}(k), \quad (7)$$

where $\mathbf{r} = \mathbf{q} - \mathbf{q}'$, $\Delta\Psi = \Psi(\mathbf{q}) - \Psi(\mathbf{q}')$, $G(k)$ is the so-called non-linear propagator $G^2(k) \approx \langle e^{i\mathbf{k}\cdot\Delta\Psi} \rangle \approx \exp(-k^2\sigma_v^2)$, and $P_{mc}(k)$ is the model-coupling contribution and σ_v^2 is the variance of the velocity. Since $P_{mc}(k)$ dominates at large k and is quite smooth, the BAO feature which could be defined as dividing $P_{nl}(k)$ by some no-wiggle template $P_{sm}(k)$, i.e.

$$\text{Wig}(k) = \frac{P_{nl}(k)}{P_{sm}(k)} - 1 \approx \exp(-k^2\sigma_v^2) \text{Wig}_{ini}(k), \quad (8)$$

would be smeared out at lower redshift and smaller scale by the bulk flow $\Delta\Psi$. Therefore, it is clear that with our reconstruction algorithm, one will no longer be affected by this smearing.

To examine the reconstructed BAO signature, we run a few N-body simulations with different transfer functions (with or without BAO, and with different s) but the same initial random seeds. This enables us to reveal the signal with little numerical efforts but free from the sample variance. As shown in the upper panel of Figure 2., at redshift $z = 0$, BAO signature becomes basically invisible after the fourth peaks (*red-dashed line*), whereas the non-linear displacement potential ϕ_{long}^{sim} (*blue-dashed*

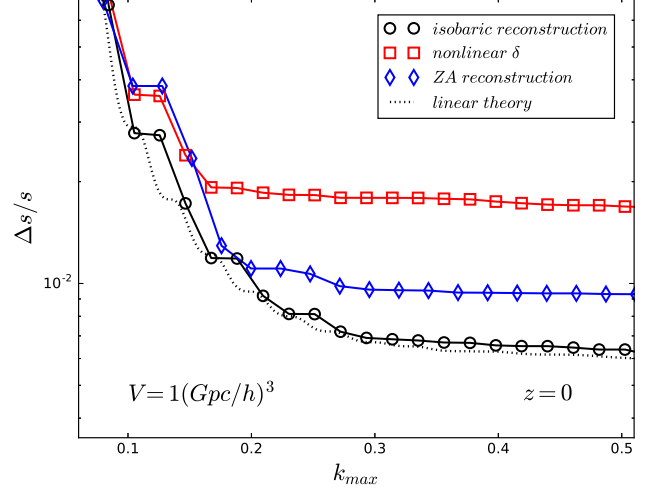


Figure 3. The fractional error of measuring the sound horizon scale $\Delta s/s$ as a function of maximum k for a noiseless survey of volume $1(\text{Gpc}/h)^3$ at redshift $z = 0$. The measurement precision after the isobaric reconstruction is very close to the linear theory, which assumes both linear power spectra and Gaussian covariance matrix (equation 11). The error after the reconstruction is roughly 2.7 times smaller than original density field, compared to a factor of ~ 1.8 smaller for the ZA reconstruction method.

line) is almost identical to the initial density field (*red-dotted line*) in this k range. The BAO of the reconstructed field ϕ^{rec} (*black-solid line*), are recovered with very high fidelity (even the eighth peak is still visible), although there does seem to exist a percent-level overall shape change. With an appropriate template, the sound horizon scale s would be recovered at a level that is very close to the linear theory, this could be seen from the numerical derivative $d \ln P(k)/d \ln s$ in the lower panel of Figure 2., which is derived from running simulations and reconstructions with slightly different s . As a comparison, we also display the performance of ZA reconstruction method (Eisenstein et al. 2007) assuming a Gaussian smoothing at $15\text{Mpc}/h$, with which the BAO is only moderately recovered.

To evaluate the impact on the constraints of the cosmic distance, we estimate the Fisher information on the sound horizon scale s for a noiseless survey. By definition, the Fisher matrix is

$$F_{\Delta \ln s} = \frac{\partial \ln P(k_i)}{\partial \ln s} C_{ij}^{-1} \frac{\partial \ln P(k_j)}{\partial \ln s}. \quad (9)$$

Here C_{ij} is the normalized covariance matrix

$$C_{ij} = \frac{1}{n_s - 1} \sum_m \left(\frac{P_m(\mathbf{k}_i)}{\langle P(\mathbf{k}_i) \rangle} - 1 \right) \left(\frac{P_m(\mathbf{k}_j)}{\langle P(\mathbf{k}_j) \rangle} - 1 \right) \quad (10)$$

which is estimated from $n_s = 200$ N-body simulations. To resemble a realistic survey, we then rescaled the large-scale component ($k < 0.1$) of matrix C_{ij} to coincide with the theoretical Gaussian covariance matrix C_{ij}^g

$$C_{ij}^g = \frac{2}{N_k} \delta_{ij}^K = \frac{4\pi^2}{k_i^2 \Delta k_i V_s} \delta_{ij}^K \quad (11)$$

assuming a survey volume of $V_s = 1 (\text{Gpc}/h)^3$, here N_k is the number of k modes of such survey.

In Figure 3., we show that the fractional error on the

sound horizon $\Delta s/s$ measured from our reconstructed field is roughly 2.7 times smaller than from the non-linear density field itself (*red dashed line*). This is very close to the accuracy one could ever achieve by measuring linear BAO (*black-dotted line*) feature and Gaussian covariance matrix. As a comparison, the same number is roughly ~ 1.8 for the ZA reconstruction.

4. DISCUSSION

As a method to get around one of the most strongest non-linearity in the structure formation process, we believe our reconstruction algorithm will significantly affect the way we measure large-scale structure in the future. However, in this paper, we did not take into account of various complications, e.g. the redshift space distortion (RSD), and the biasing. In redshift space, it would be quite straightforward to express the reconstructed field as a combination with original displacement with peculiar velocity $\Psi_{rsd} = \Psi + \mathbf{v}/\mathcal{H}$, and would be relative easy to recover Ψ by performing some Wiener filter after the reconstruction.

The biasing, on the other hand, is much more challenging, because unlike RSD the filter itself would then depend on the galaxies type. Most naively, one could simply fix the bias parameters from the unconstructed density field, e.g. via HOD fitting or simply linear bias (Padmanabhan et al. 2012). Alternatively, without any preprocessing, one could also perform the reconstruction for the biased density field itself. In this case, the reconstructed potential field ϕ_b^{rec} will not be the same as the real displacement of these tracers anymore, but instead will also include the information of their formation as well (Wang & Pen 2017).

REFERENCES

- Aleksandrov, A. D. 1958, Vestnik Leningrad. Univ. Ser. Mat. Meh. Astr., 13, 5
- Bakelman, I. J. 1957, Dokl. Akad. Nauk SSSR (N.S.), 114, 1143
- Blake, C., & Glazebrook, K. 2003, ApJ, 594, 665
- Brenier, Y., Frisch, U., H  non, M., et al. 2003, MNRAS, 346, 501
- Chan, K. C. 2014, Phys. Rev. D, 89, 083515
- Crocce, M., & Scoccimarro, R. 2006, Phys. Rev. D, 73, 063519
- Crocce, M., & Scoccimarro, R. 2008, Phys. Rev. D, 77, 023533
- Croft, R. A. C., & Gaztanaga, E. 1997, MNRAS, 285, 793
- Eisenstein, D. 2003, ArXiv Astrophysics e-prints, astro-ph/0301623
- Eisenstein, D. J., Seo, H.-J., Sirko, E., & Spergel, D. N. 2007, ApJ, 664, 675
- Eisenstein, D. J., Zehavi, I., & Hogg, e. a. 2005, ApJ, 633, 560
- Gramann, M. 1993, ApJ, 405, 449
- Hu, W., & Haiman, Z. 2003, Phys. Rev. D, 68, 063004
- Lions, P. L., Trudinger, N. S., & Urbas, J. I. E. 1986, Comm. Pure Appl. Math., 39, 539
- Liu, J., Froese, B. D., Oberman, A. M., & Xiao, M. 2014, ArXiv e-prints, arXiv:1411.7018
- Mehta, K. T., Cuesta, A. J., Xu, X., Eisenstein, D. J., & Padmanabhan, N. 2012, MNRAS, 427, 2168
- Narayanan, V. K., & Croft, R. A. C. 1999, ApJ, 515, 471
- Neyrinck, M. C. 2011, ApJ, 742, 91
- Ngan, W., Harnois-D  raps, J., Pen, U.-L., McDonald, P., & MacDonald, I. 2012, MNRAS, 419, 2949
- Nusser, A., & Dekel, A. 1992, ApJ, 391, 443
- Padmanabhan, N., Xu, X., Eisenstein, D. J., et al. 2012, MNRAS, 427, 2132
- Pan, Q., Pen, U.-L., Inman, D., & Yu, H.-R. 2016, ArXiv e-prints, arXiv:1611.10013
- Peebles, P. J. E. 1989, ApJ, 344, L53
- Peebles, P. J. E. 1990, ApJ, 362, 1
- Pen, U.-L. 1995, ApJS, 100, 269
- Pen, U.-L. 1998, ApJS, 115, 19
- Planck Collaboration, Ade, P. A. R., Aghanim, N., et al. 2016, A&A, 594, A13
- Rimes, C. D., & Hamilton, A. J. S. 2005, MNRAS, 360, L82
- Rimes, C. D., & Hamilton, A. J. S. 2006, MNRAS, 371, 1205
- Schmittfull, M., Feng, Y., Beutler, F., Sherwin, B., & Chu, M. Y. 2015, Phys. Rev. D, 92, 123522
- Seo, H.-J., & Eisenstein, D. J. 2003, ApJ, 598, 720
- Seo, H.-J., & Eisenstein, D. J. 2007, ApJ, 665, 14
- Tassev, S., & Zaldarriaga, M. 2012a, JCAP, 12, 011
- Tassev, S., & Zaldarriaga, M. 2012b, JCAP, 10, 006
- Trudinger, N. S., & Wang, X.-J. 2008, The Monge-Amp  re equation and its geometric applications, Vol. 1 (International Press), 467–524
- Wang, H., Mo, H. J., Yang, X., & van den Bosch, F. C. 2013, ApJ, 772, 63
- Wang, X., & Pen, U.-L. 2017, *in prep.*
- Weinberg, D. H. 1992, MNRAS, 254, 315
- Yu, Y., Zhu, H.-M., & Pen, U.-L. 2017, arXiv:1703.08301
- Zheligovsky, V., Podvigina, O., & Frisch, U. 2010, Journal of Computational Physics, 229, 5043
- Zhu, H.-M., Yu, Y., Pen, U.-L., Chen, X., & Yu, H.-R. 2016, ArXiv e-prints, arXiv:1611.09638